Author Manuscript

Author Manuscript

Author Manuscript

Author Manuscript

HHS Public Access

Author manuscript

Ann Biomed Eng. Author manuscript; available in PMC 2018 March 01.

Published in final edited form as:

Ann Biomed Eng. 2017 March ; 45(3): 819–828. doi:10.1007/s10439-016-1724-1.

Effects of Iron on Physical and Mechanical Properties, and Osteoblast Cell Interaction in β-Tricalcium Phosphate

Sahar Vahabzadeh and **Susmita Bose***

W. M. Keck Biomedical Materials Research Laboratory, School of Mechanical and Materials Engineering, Washington State University, Pullman, WA 99164-2920, USA, Tell: (509) 335-7461, Fax: (509) 335-4662

Abstract

Iron (Fe) is a vital element and its deficiency causes abnormal bone metabolism. We investigated the effects of Fe and its concentration in β-tricalcium phosphate (β-TCP) on physicomechanical properties and *in vitro* proliferation and differentiation of osteoblasts. Our results showed that Fe addition at concentrations of 0.5 wt. % (0.5 Fe-TCP) and 1.0 wt. % (1.0 Fe-TCP) inhibits the β-TCP to α-TCP phase transformation at sintering temperature of 1250 °C. Addition of 0.25 wt. % Fe (0.25 Fe-TCP) increased the compressive strength of β-TCP from 167.27±16.2 MPa to 227.10±19.3 MPa. After 3 days of culture, surfaces of 0.5 Fe-TCP and 1.0 Fe-TCP samples were covered by osteoblast cells, compared to that of pure and 0.25 Fe-TCP. Cells grew to confluency on all Fe-doped samples after 7 days of culture and monolayer sheetlike cellular structure was found at 11 days. Optical cell density and alkaline phosphatase activity were significantly higher on Fe-doped samples and the highest values were found in 0.5 Fe-TCP samples. Our results show that Fe concentration had significant effect on physical and mechanical properties of TCP ceramics, and also on the *in vitro* osteoblast cellular interactions in TCP ceramics.

Keywords

Phase transformation; compressive strength; iron dopant; proliferation and differentiation of osteoblast cells

1.0 Introduction

Osteoporosis, characterized by significant decrease in bone mineral density (BMD) and bone quality, is considered as one of the most common bone diseases that can lead to higher risk of bone fracture. [57] Most osteoporotic bone fractures occur in the forearm, humerus, hip, vertebrae and spine. [22,58] Worldwide, more than 8.9 million fractures are caused by osteoporosis, annually. [58] In 2014, the National Osteoporosis Foundation (NOF) announced that a total of 54 million Americans above the age of 50 are suffering from osteoporosis and this number will increase to 64.4 million by 2020. [59]. In addition, the medical costs of osteoporosis are approximated to be $22 billion, annually.[27] Increasing life expectancy requires new approaches to decrease the rate of osteoporosis and reverse the bone loss.

*Corresponding author: sbose@wsu.edu.

Author Manuscript Author Manuscript Author Manuscript Author Manuscript

Calcium phosphate (CaP) based ceramics are being widely used in bone tissue engineering due to their osteoconductivity and compositional similarity to that of bone. [35] Despite being osteoconductive, calcium phosphate ceramics (CPCs) have negligible osteoinduction. [40] One of the promising solutions to enhance the osteoinduction of CPCs *in vitro* and *in vivo* is the addition of trace elements such as Si, Zn, Li, Mg, Mn and Sr. [4,8,9,15,18,21,23,39,43,44] Iron (Fe) is a vital material and its deficiency is known to cause abnormal bone metabolism. [26,30] In addition, Fe plays a crucial role in vitamin D metabolism, and synthesis and maturation of collagen. [25,29] In specific case such as thalassemia, iron overload can cause severe osteoporosis and osteoporotic bone fractures. [49] In the current work, we have studied the effects of Fe and its concentration in TCP on physical and mechanical properties, and also on *in vitro* osteoblast cell interactions. Although multiple reports are available on the effects of dietary iron on overall bone metabolism and collagen synthesis, [1,20,25,26,33] there are a few studies on the interaction between bone cells and calcium phosphate-coated iron nanoparticles. [34,46] We hypothesize that presence of Fe alters the physical and mechanical properties of TCP samples, and changes the *in vitro* osteoblast cell responses.

Two forms of iron oxides, maghemite (Fe_2O_3) and magnetite (Fe_3O_4) nanoparticles, are of great interest in biomedical applications such as magnetic resonance imaging (MRI), cancer hyperthermia, *in vitro* cell separation, and targeted drug delivery. [11,17,19,28,36] However, the use of magnetic nanoparticles in CaP scaffolds for bone tissue engineering applications is rarely reported. In the current work, Fe_2O_3 nanoparticles with the size of <50 nm were added to TCP precursors to achieve the Fe-doped TCP scaffolds.

We hypothesize that the amount of Fe dopant affects the phase transformation, porosity, compressive strength, and *in vitro* osteoblast cell-material interaction in TCP samples. To validate our hypothesis, we report the effects of different Fe concentration on the phase composition of TCP samples, sintered at 1250 °C. Samples were made by solid state synthesis method followed by uniaxial pressing. We investigated the effects of Fe concentration on the porosity and the compressive strength of the TCP samples using Archimedes' method and uniaxial compression test, respectively. To understand *in vitro* bone cell material interactions, we studied the effects of Fe concentration on proliferation and differentiation of osteoblast cell using the SEM, MTT and ALP assays. To the best of our knowledge, there is no study on effects of Fe on physical and mechanical properties of TCP, as well as on the *in vitro* osteoblast cell interaction in TCP ceramics.

2.0 Materials and Methods

2.1 Pure and Doped TCP Synthesis

Pure and Fe-doped β-tricalcium phosphate powders (β-TCP) were synthesized via solid state method. 1 mole calcium carbonate ($CaCO_3$) and 2 moles dicalcium phosphate ($CaHPO_4$) were mixed and ball milled for 2 hours, followed by calcinations at 1050 °C for 24 hours. High purity iron oxide (Fe_2O_3, < 50 nm, Sigma-Aldrich) was added to TCP precursors to obtain 0.25, 0.5, and 1 wt. % Fe-doped TCP. Calcined powders were then crushed and mixed with ethanol at an ethanol: powder ratio of 1.5:1.0. The mixtures were then milled for 6 h at 70 rpm, followed by drying at 70 °C. Dried powders were pressed into disks (12 mm diameter and 2 mm thickness) for phase analysis, micrograph investigation and cell culture

Author Manuscript Author Manuscript Author Manuscript Author Manuscript

study using a uniaxial press, followed by cold isostatic pressing at 413 MPa. Similarly, cylindrical samples (7 mm diameter and 12 mm height) were prepared for density and compressive strength measurements. Finally, all the pressed samples were sintered at 1250 °C in a muffle furnace for 2 h. From now on, 0, 0.25, 0.5, and 1.0 wt. % Fe doped β-TCP samples will be denoted as pure TCP, 0.25 Fe-TCP, 0.5 Fe-TCP and 1.0 Fe-TCP, respectively.

2.2 Phase Analysis, Microstructure Analysis, and Mechanical Properties

Phase analysis of pure and Fe doped samples was performed using X-ray diffractometer (XRD) with a Siemens D500 Kristalloflex system (Siemens D500 Kristalloflex, Madison, WI) with Cukα radiation over 2θ values of 20–60° at the step size of 0.05° and a count time of 0.1 sec per step. Relative intensity ratio of major peaks of β-TCP and α-TCP was used to calculate the percentages of these two phases in the samples as described elsewhere.[48]

Field emission scanning electron microscope (FESEM, FEI 200F, FEI Inc., OR, USA) was used to characterize the surface morphology of sintered samples. Bulk density and total porosity of disk samples were measured using their mass and physical dimensions (Total porosity % = 100-relative bulk density). Relative apparent density, closed porosity, and open porosity were measured using Archimedes' method. Samples were submerged in boiling water for 3 minutes and then transferred to water at room temperature where the wet weight was measured. Density and porosity values were obtained by taking the average of measurements for 4 samples. Compressive strength of cylindrical samples was measured using a screw-driven Instron testing machine (AG-IS, Shimadzu, Tokyo, Japan). Compressive strength was calculated using the maximum load at failure and sample dimensions. Compressive strength was obtained by averaging the compressive strengths of 7–10 samples.

2.3 In Vitro Human Fetal Osteoblast Culture

All samples were sterilized at 121°C for 20 minutes prior to cell culture using an autoclave. Human fetal osteoblast cells (hFOB 1.19, ATCC, Manassas, VA) were seeded on the disks with the density of 3×10^4 cells/40 μl per sample at passage 3. Followed by incubation at 34 °C and primary cell adhesion, the filter sterilized base medium, Dulbecco's Modified Eagle's Medium/Nutrient Mixture F-12 Ham (DMEM/F12, Sigma, St. Louis, MO), with 2.5 mM L-glutamine (without phenol red), supplemented with 300 mg L^{-1} G418 (Sigma) and 10% fetal bovine serum (FBS, Sigma) was added to wells. Cultures were maintained at 34 °C under an atmosphere of 5% CO_2/95% air and cell medium was changed with fresh medium every 2–3 days during the culture experiment.

2.4 Cellular Morphology, MTT and ALP Assays

To study the cellular morphology using FESEM, samples were removed from the culture at 3, 7, and 11 days and fixed with 2% paraformaldehyde/2% glutaraldehyde in 0.1 M phohsphate buffer at 4 °C overnight. Samples were rinsed with 0.1 M phosphate buffer three times, followed by post fixation with 1 % osmium tetroxide (OsO_4) overnight at 4 °C. Samples were then rinsed again with 0.1 M phosphate buffer three times and dehydrated in

Author Manuscript Author Manuscript Author Manuscript Author Manuscript

graduated ethanol series (30, 50, 70, 95, and 100 % three times), followed by hexamethyldisilane (HMDS) drying procedure.

MTT (3-(4,5-dimethylthiazol-2-yl)-2,5-diphenyl tetrazolium bromide) assay was used to evaluate osteoblast cell viability after 3, 7, and 11 days of culture. The MTT (Sigma, St. Louis, MO) solution of 5 mg mL-1 was prepared by dissolving MTT powder in filter sterilized PBS. 100 μL of MTT solution was added dropwise on top of each sample in well plate, followed by addition of 900 μL cell medium. Samples were then incubated at 34 °C for 2 h. The medium was then removed and 500 μL of solution (composed of 10 % Triton X-100, 0.1N HCl and isopropanol) was added to each sample to dissolve formazan crystals. 100 μL of solution in triplicate was transferred to 96-well plate and read by UV–Vis spectroscopy (BioTek) at 570 nm.

Differentiation of osteoblast cell was evaluated using colorimetric alkaline phosphatase (ALP) assay kit (abcam, Cambridge, MA) according to the protocol from the provider. Briefly, osteoblast cells were detached from surface of samples using Trypsin-EDTA solution (ATCC), followed by centrifuging at 1000 rpm and removing the supernatant. Then 400 μL of assay buffer solution was added to each sample and the solution was centrifuged to remove the insoluble material at 13000 rpm for 3 min. 80 μL of samples was transferred to 96 well plates in triplicate and 50 μL of the 5 mM *p*-nitrophenyl phosphate (*p*NPP) solution was added. Samples were incubated at 25 °C for 1 h and then, 20 μL of stop solution was added to each well. The optical density was measured at 405 nm using UV–Vis spectroscopy.

2.5 Statistical Analysis

Data for relative bulk density, relative apparent density, compressive strength, MTT and ALP assays are presented as mean ± standard deviation. Statistical analysis was performed on the data using student's t-test, and P values < 0.05 and <0.01 were considered as significant and very significant, respectively.

3.0 Results

3.1 Phase Analysis and Microstructure

Figure 1 shows the XRD spectra of pure and Fe doped samples after sintering at 1250 °C. Spectra of all samples showed the β-TCP (JCPDS No. 09-169) as the major phase. α-TCP peaks (JCPDS No. 09-0348) were also present in pure and 0.25 Fe-TCP samples; however, no α-TCP peaks were found in samples with higher concentrations of Fe.

Microstructure of samples is presented in Figure 2. FESEM micrographs show a dense structure for all compositions. Granular structure in pure and 0.25 Fe-TCP was clearly visible and addition of 0.25 wt. % Fe increased the particle size of TCP from 4.1±2.4 μm to 5.3±2.1 μm. Compared to pure and 0.25 Fe-TCP samples, partial liquid phase sintering was observed in 0.5 Fe-TCP. Increasing the concentration of dopant to 1.0 wt. % resulted in forming extensive liquid phase with negligible amount of open porosity.

Author Manuscript Author Manuscript Author Manuscript Author Manuscript

3.2 Density Measurement and Mechanical Properties

Relative bulk and apparent densities of samples were measured using the dimension of samples and Archimedes' method. As shown in Figure 3a, addition of 0.25 wt. % Fe increased the relative bulk density of TCP from 80.33±1.3 % to 87.92±0.6 %. Relative bulk density of 0.5 and 1.0 Fe-TCP samples were 90.06±0.6 % and 93.10±0.3 %, respectively. Relative apparent density was in the range of 90–96 % for all samples, regardless of their composition.

Compressive strength data of pure and Fe-doped TCP samples are presented in Figure 3b. Addition of 0.25 wt. % Fe increased the compressive strength of β-TCP significantly from 167.27±16.2 MPa to 227.10±19.3 MPa. However, addition of higher amounts of Fe did not result in further increase in compressive strength. Compressive strength was 235.19±25.7 MPa and 219.75±36.1 MPa for 0.5 and 1.0 Fe-TCP samples, respectively.

3.3 Cellular Morphology, Proliferation, and Differentiation

To understand cell-material interaction, the morphology of the osteoblast cells on pure and doped samples was analyzed using FESEM after 3, 7, and 11 days of culture (Figure 4). Cells were well attached to all the samples after 3 days. Compared to pure and 0.25 Fe-TCP, much more cells were attached to 0.5 and 1.0 Fe-TCP. After 7 days of culture, quite a few cells were found on pure and Fe doped TCPs. However, cells reached to the confluent monolayer on all Fe doped samples, regardless of Fe concentration. Compared to day 7, cell density increased on pure TCP after 11 days of culture. The surfaces of all doped samples were covered with osteoblast cells, resembling multiple layer features.

Proliferation of osteoblast cells on pure and Fe-doped TCP samples was determined using MTT assay. Figure 5 presents the optical cell density after 3, 7, and 11 days of culture. At day 3, the optical cell density was statistically higher on all doped samples compared to the pure TCP. The cell density increased significantly on all doped samples from day 3 to day 7. The highest optical cell density at day 7 was found on 0.5 Fe-TCP. At day 11, cell proliferation increased on all samples regardless of the presence of Fe dopant and its concentration; however, the cell density was again the highest on 0.5 Fe-TCP.

ALP assay was used to evaluate the differentiation of osteoblast cells on samples after 7 and 11 days of culture. Figure 6 shows the effects of Fe concentration on ALP activity. At day 7 of culture, all doped samples had significantly higher ALP activity compared to the pure TCP. Among different Fe concentrations, 0.5 Fe-TCP showed the highest osteoblast differentiation at day 7. ALP activity increased for all samples after 11 days and the difference between the doped samples was less noticeable than that of day 7.

4.0 Discussion

Tricalcium phosphates (TCPs) are of great interest as bone substitutes for non-load bearing applications due to their bioactivity and similarity to the composition of bone. Though osteoconductive, lack of osteoinduction is the main drawback for using TCPs as bone substitute materials for enhanced osteogenesis and/or angiogenesis. Addition of trace elements is a feasible alternative to enhance the osteoconductivity and osteoinductivity of

Author Manuscript Author Manuscript Author Manuscript Author Manuscript

TCPs. Trace elements such as Na, Mg, Sr, Zn, Fe, Al, Ag, Mn, Cr, Si, and Br are present in enamel, dentine or bone. [6] The effects of Na, Mg, Sr, Zn, Ag, Mn, Si on physical, mechanical, *in vitro* and/or *in vivo* properties of CaPs is well reported. [9,12,13,18,21,23,37,38,41] Fe is a vital material and plays critical role in bone metabolism. [26,30] In this study, we have investigated the effects of Fe^{3+} and its concentration on physical and mechanical properties of TCP. Pure and Fe-doped TCP powders were synthesized through solid state route and pressed to disk shapes, followed by sintering at 1250 °C. Then, attachment, proliferation and differentiation of human fetal osteoblast cells were studied as a function of Fe concentration.

Present results show that not only does Fe^{3+} impact the phase composition, and compressive strength of TCP ceramics; but also it improves their interactions with osteoblast cells. Addition of Fe^{3+} retards the β-TCP to α-TCP phase transformation. β-TCP is the stable phase up to 1125 °C and at temperatures between 1125 °C and 1430 °C, α-TCP becomes stable.[53] As a result, presence of α-TCP is expected at sintering temperature of 1250 °C. Presence of β-TCP as a single phase in samples with high Fe concentration (0.5 and 1.0 wt. %) shows the inhibitory effect of Fe on β to α-TCP phase transformation. Thermal stability of β-TCP at high temperature is related to the stabilization of the crystal structure by the ionic substitution and lattice contraction. [24] Trivalent metal ions substitute at the calcium ion sites and vacancies. [54] The ionic radius of Ca^{2+} and Fe^{3+} is 0.99 Å and 0.64 Å, respectively. As a result, substitution of Ca^{2+} with Fe^{3+} decreases the unit cell size of β-TCP and thus, increases the β-TCP phase stability. β-TCP to α-TCP phase transformation is an important phenomenon in bone regeneration. Though both phases are bioactive, higher solubility product of α-TCP (3.16×10^{-26}) as compared to that of β-TCP (1.25×10^{-29}) results in its faster degradation rate in biological environment and substitution with bone.[35] It is important to mention that Fe^{3+} addition to hydroxyapatite (HAP) structure using mechanical milling for 20 h results in the formation of $Ca_2Fe_2O_5$ with brownmillerite crystal structure, indicating the reaction between HAP and Fe_2O_3, which is in contrast to our findings where no reaction between iron oxide and tricalcium phosphate was found.[16,42]

Addition of Fe^{3+} to TCP is accompanied by grain growth and liquid phase formation. According to the phase diagram in the Fe_2O_3-P_2O_5 system, several liquid phases including $Fe(PO_3)_3$ (JCPDS # 44-0772), $Fe_4(P_2O_7)_3$ (JCPDS # 36-0318), $FePO_4$ (JCPDS # 84-0875), and Fe_3PO_7 (JCPDS# 37-0061) may form in temperature range from 907±8 °C to 1208±8 °C. [56] However, no peak related to these phases was found in the XRD spectra of samples, most likely due to the low amount of Fe_2O_3.

Addition of iron results in a significant increase in relative bulk and apparent densities of TCP. Increase in the bulk density is related to the decrease in the unit cell volume during Fe^{3+} substitution in Ca^{2+} site. This behavior proves the effective role of Fe dopant on decreasing the total and open porosities. These findings are in line with SEM micrographs (Figure 2) where significantly less open pores are present in the doped samples, most notably in 1.0 Fe-TCP, as compared to pure TCP.

Compressive strength of ceramic samples is mainly affected by phase composition, particle size, density, and liquid phase sintering. Formation of phases with higher strength, decrease in particle size, and increase in density are usually accompanied with enhancement of

Author Manuscript Author Manuscript Author Manuscript Author Manuscript

compressive strength. On the other hand, extensive liquid phase formation drops the mechanical strength of final product. [10] Addition of 0.25 wt. % Fe increases the bulk and apparent densities and slightly decreases the α-TCP phase content which results in significant increase in compressive strength of pure TCP from 167.27±16.2 MPa to 227.10±19.3 MPa. Though addition of higher amounts of Fe up to 1.0 wt. % inhibits the α-TCP phase formation and increases the density, large amount of liquid phase causes the decrease in compressive strength. These results effectively highlight the contradictory effects of Fe on enhancement of strength in TCP.

To evaluate the efficacy of Fe-doped TCP samples as bone substitute materials, the *in vitro* interaction between human fetal osteoblast cell and samples was investigated. Iron is an important element in the body and its deficiency causes severe health problems such as anemia, changes in vitamin metabolism, and also abnormal bone metabolism. In addition, dietary iron deficiency compromises the bone mineral density (BMD), bone mineral content (BMC), and mechanical strength. Iron is also an important factor in vitamin D metabolism and collagen synthesis and maturation. [25,26,29,30] Katsumata *et al.* found that iron deficiency causes the calcium and protein deficiency; both play an important role in bone metabolism. It also decreases the osteocalcin concentration which inhibits bone formation. [25,26] In addition to the decrease in bone formation, lack of iron compromises the bone resorption *in vivo*. Due to the elevated decrease in osteoclastogenesis, the overall bone loss occurs in an iron-deficient diet. [25,30] On the other hand, iron overload in specific cases such as thalassemia causes osteoporosis and bone fracture. Excess amounts of iron causes the abnormalities in bone phenotype, cortical and trabecular thinning and changes in bone composition, depending on the Fe dose. These controversies show the importance of regulating the iron amount on bone formation and/or resorption. [47,49] Our data support the expected effects of Fe as a dopant in TCP structure on proliferation and differentiation of osteoblast cells. Results shown in Figure 4 present good adhesion of osteoblasts on all samples, with larger number of cells on doped samples at day 3 of culture. Cell adhesion is the primary stage which directly alters the proliferation and differentiation behavior at later stages. The MTT assay results also show higher number of cells on Fe-doped samples which is in line with the SEM results. After 7 days of culture, the surfaces of doped samples were almost entirely covered by osteoblast cells. Cells grew to confluency on all doped samples resembling a multilayer structure covered by abundant filopodia extensions after 11 days of culture. These results are in line with the MTT assay findings which showed 2-3 fold increase in cell density on Fe-doped samples compared to that of control pure TCP samples. Previous reports showed the cytocompatibility of Fe-doped calcium phosphate glass fiber composites in the presence of preosteoblast cells. In addition, magnetic nanoparticles enhance the *in vitro* proliferation of osteoblasts. [31,32,34,52] The enhanced proliferation of osteoblast cells is also reported in TCP scaffolds, doped with other elements such as Li, Zn, Mg, Sr, Mg/Zn, and Sr/Zn. [2,3,14,48] The overall trend of proliferation of osteoblast cells is similar to our previous studies, e.g. Li, Fe, Zn, and Mg/Zn doped TCP samples.[2,48] Along with proliferation, differentiation is another important stage that determines the final fate of osteoblasts: osteocyte, bone lining cell, or apoptosis. [7] ALP is an important enzyme that is released during the maturation of osteoblast cells, providing an alkaline environment that favors new bone formation. This enzyme is also a marker for differentiation of osteoblast

Author Manuscript Author Manuscript Author Manuscript Author Manuscript

cells. [5] ALP assay results show 2-6 fold increase in osteoblast differentiation on all doped samples at day 7 of culture. Increase in ALP expression on all samples after 11 days indicates the ongoing differentiation; however, 0.5 Fe-TCP shows the least upregulation of ALP. Controversies of iron effects on differentiation of osteoblast cells require a deeper understanding of its role in each system. Few *in vitro* and *in vivo* studies have indicated the inhibitory effect of iron on osteoblast differentiation through downregulation of osteogenic markers such as BMP-2, RUNX-2, and osteocalcin. [52] However, other reports have shown that the dose dependency of enhancement in osteoblast cell proliferation and differentiation in magnetic CaPs, mainly superparamagnetic nanoparticles due to increase in fibronectin adsorption, ALP expression and collagen synthesis. [34,45,46] Increase in bone density and decrease in osteoporosis, in presence of magnetic field has been already reported. Proliferation and differentiation of osteoblast cells and upregualtion of BMPs under exposure to magnetic fields result in enhanced osteointegration and new bone formation *in vivo.* [50,51] It has also been reported that applying external mechanical force to bone could generate an electric field, leading to response from the bone cells to physical stimuli, due to the piezoelectric property of bone. [51,55] Figure 7 summarizes the results from this study and correlates them with the literature. Presence of Fe and magnetic field enhance the fibronectin adsorption, [45,46,50] and facilitate the proliferation and differentiation of osteoblast cells. These primary results show the effects of iron as a dopant on physical and mechanical properties of TCP, along with *in vitro* osteoblast cell interaction with TCP.

5.0 Conclusion

Here we report the effects of Fe and its concentration on physical, mechanical, and *in vitro* osteoblast cell-material interaction in TCP samples. Fe addition at concentrations of 0.5 and 1.0 wt. % inhibited the β-TCP to α-TCP phase transformation at 1250 °C, and led to liquid phase formation. Addition of 0.25 wt. % Fe increased the compressive strength of β-TCP from 167.27±16.2 MPa to 227.10±19.3 MPa and higher concentrations of Fe did not change the compressive strength, significantly. In addition, presence of Fe increased both relative bulk and apparent densities. Proliferation and differentiation of osteoblast cells were enhanced in all doped samples and the highest activity was found in samples doped with 0.5 wt. % Fe. These data were in line with the SEM results, where multilayer cellular structure was found in doped samples at 11 days of culture. Though further research is needed for deeper understanding of Fe role in bone remodeling process, the present results show the potential use of Fe-doped TCP in bone tissue engineering applications.

Acknowledgments

The authors would like to acknowledge financial support from the National Institute of Health (NIAMS-R01-AR-066361). The authors also thank the Franceschi Microscopy and Imaging Center at Washington State University.

References

1. Abraham R, Walton J, Russell L, Wolman R, Wardley-Smith B, Green JR, Mitchell A, Reeve J. Dietary determinants of post-menopausal bone loss at the lumbar spine: a possible beneficial effect of iron. Osteoporos Int J Establ Result Coop Eur Found Osteoporos Natl Osteoporos Found USA. 2006; 17:1165–1173.

Author Manuscript Author Manuscript Author Manuscript Author Manuscript

2. Bandyopadhyay A, Bernard S, Xue W, Bose S. Calcium Phosphate-Based Resorbable Ceramics: Influence of MgO, ZnO, and SiO2 Dopants. J Am Ceram Soc. 2006; 89:2675–2688.
3. Bandyopadhyay A, Petersen J, Fielding G, Banerjee S, Bose S. ZnO, SiO2, and SrO doping in resorbable tricalcium phosphates: Influence on strength degradation, mechanical properties, and in vitro bone-cell material interactions. J Biomed Mater Res B Appl Biomater. 2012; 100:2203–2212. [PubMed: 22997062]
4. Banerjee SS, Tarafder S, Davies NM, Bandyopadhyay A, Bose S. Understanding the influence of MgO and SrO binary doping on the mechanical and biological properties of β-TCP ceramics. Acta Biomater. 2010; 6:4167–4174. [PubMed: 20493283]
5. Bilezikian, JP., Raisz, LG., Martin, TJ. Principles of Bone Biology. Cambridge: Academic Press; 1900.
6. Boanini E, Gazzano M, Bigi A. Ionic substitutions in calcium phosphates synthesized at low temperature. Acta Biomater. 2010; 6:1882–1894. [PubMed: 20040384]
7. Bose S, Fielding G, Tarafder S, Bandyopadhyay A. Understanding of dopant-induced osteogenesis and angiogenesis in calcium phosphate ceramics. Trends Biotechnol. 2013; 31:594–605. [PubMed: 24012308]
8. Bose S, Tarafder S, Banerjee SS, Davies NM, Bandyopadhyay A. Understanding In Vivo Response and Mechanical Property Variation in MgO, SrO and SiO2 doped β-TCP. Bone. 2011; 48:1282–1290. [PubMed: 21419884]
9. Bracci B, Torricelli P, Panzavolta S, Boanini E, Giardino R, Bigi A. Effect of Mg2+, Sr2+, and Mn2+ on the chemico-physical and in vitro biological properties of calcium phosphate biomimetic coatings. J Inorg Biochem. 2009; 103:1666–1674. [PubMed: 19819556]
10. Carter, CB., Norton, MG. Ceramic Materials. New York, NY: Springer New York; 2013. p. 766at <http://link.springer.com/10.1007/978-1-4614-3523-5>
11. Ciobanu CS, Iconaru SL, Gyorgy E, Radu M, Costache M, Dinischiotu A, Le Coustumer P, Lafdi K, Predoi D. Biomedical properties and preparation of iron oxide-dextran nanostructures by MAPLE technique. Chem Cent J. 2012; 6:17. [PubMed: 22410001]
12. DeVoe K, Banerjee S, Roy M, Bandyopadhyay A, Bose S. Resorbable Tricalcium Phosphates for Bone Tissue Engineering: Influence of SrO Doping. J Am Ceram Soc. 2012; 95:3095–3102.
13. Ewald A, Hösel D, Patel S, Grover LM, Barralet JE, Gbureck U. Silver-doped calcium phosphate cements with antimicrobial activity. Acta Biomater. 2011; 7:4064–4070. [PubMed: 21763795]
14. Fielding GA, Smoot W, Bose S. Effects of SiO2, SrO, MgO, and ZnO dopants in tricalcium phosphates on osteoblastic Runx2 expression. J Biomed Mater Res A. 2014; 102:2417–2426. [PubMed: 23946240]
15. Fielding G, Bose S. SiO2 and ZnO dopants in three-dimensionally printed tricalcium phosphate bone tissue engineering scaffolds enhance osteogenesis and angiogenesis in vivo. Acta Biomater. 2013; 9:9137–9148. [PubMed: 23871941]
16. Filho FP, Nogueira REFQ, Graça MPF, Valente MA, Sombra ASB, Silva CC. Structural and mechanical study of the sintering effect in hydroxyapatite doped with iron oxide. Phys B Condens Matter. 2008; 403:3826–3829.
17. Gupta AK, Gupta M. Synthesis and surface engineering of iron oxide nanoparticles for biomedical applications. Biomaterials. 2005; 26:3995–4021. [PubMed: 15626447]
18. Han P, Xu M, Chang J, Chakravorty N, Wu C, Xiao Y. Lithium release from β-tricalcium phosphate inducing cementogenic and osteogenic differentiation of both hPDLCs and hBMSCs. Biomater Sci. 2014; 2:1230–1243.
19. Hardouin J, B F. PEGylated Versus Non-PEGylated γ Fe2O3@Alendronate Nanoparticles. J Bioanal Biomed. 2012; 4
20. Harris MM, Houtkooper LB, Stanford VA, Parkhill C, Weber JL, Flint-Wagner H, Weiss L, Going SB, Lohman TG. Dietary iron is associated with bone mineral density in healthy postmenopausal women. J Nutr. 2003; 133:3598–3602. [PubMed: 14608080]
21. Hing KA, Revell PA, Smith N, Buckland T. Effect of silicon level on rate, quality and progression of bone healing within silicate-substituted porous hydroxyapatite scaffolds. Biomaterials. 2006; 27:5014–5026. [PubMed: 16790272]

Author Manuscript Author Manuscript Author Manuscript Author Manuscript

22. Hopkins RB, Tarride JE, Leslie WD, Metge C, Lix LM, Morin S, Finlayson G, Azimaee M, Pullenayegum E, Goeree R, Adachi JD, Papaioannou A, Thabane L. Estimating the excess costs for patients with incident fractures, prevalent fractures, and nonfracture osteoporosis. Osteoporos Int. 2013; 24:581–593. [PubMed: 22572964]
23. Ito A, Kawamura H, Otsuka M, Ikeuchi M, Ohgushi H, Ishikawa K, Onuma K, Kanzaki N, Sogo Y, Ichinose N. Zinc-releasing calcium phosphate for stimulating bone formation. Mater Sci Eng C. 2002; 22:21–25.
24. Kannan S, Goetz-Neunhoeffer F, Neubauer J, Pina S, Torres PMC, Ferreira JMF. Synthesis and structural characterization of strontium- and magnesium-co-substituted beta-tricalcium phosphate. Acta Biomater. 2010; 6:571–576. [PubMed: 19679202]
25. Katsumata S, Katsumata-Tsuboi R, Uehara M, Suzuki K. Severe iron deficiency decreases both bone formation and bone resorption in rats. J Nutr. 2009; 139:238–243. [PubMed: 19106323]
26. Katsumata S, Tsuboi R, Uehara M, Suzuki K. Dietary iron deficiency decreases serum osteocalcin concentration and bone mineral density in rats. Biosci Biotechnol Biochem. 2006; 70:2547–2550. [PubMed: 17031035]
27. Lee D, Filler B, Twetten M. Enhancing Fracture and Osteoporosis Care. AAOS Now. 7:30.
28. Lodhia J, Mandarano G, Ferris N, Eu P, Cowell S. Development and use of iron oxide nanoparticles (Part 1): Synthesis of iron oxide nanoparticles for MRI. Biomed Imaging Interv J. 2010; 6:e12. [PubMed: 21611034]
29. McGillivray G, Skull SA, Davie G, Kofoed SE, Frydenberg A, Rice J, Cooke R, Carapetis JR. High prevalence of asymptomatic vitamin D and iron deficiency in East African immigrant children and adolescents living in a temperate climate. Arch Dis Child. 2007; 92:1088–1093. [PubMed: 17768148]
30. Medeiros DM, Plattner A, Jennings D, Stoecker B. Bone morphology, strength and density are compromised in iron-deficient rats and exacerbated by calcium restriction. J Nutr. 2002; 132:3135–3141. [PubMed: 12368407]
31. Mohammadi MS, Ahmed I, Muja N, Almeida S, Rudd CD, Bureau MN, Nazhat SN. Effect of Si and Fe doping on calcium phosphate glass fibre reinforced polycaprolactone bone analogous composites. Acta Biomater. 2012; 8:1616–1626. [PubMed: 22248526]
32. Panseri S, Cunha C, D'Alessandro T, Sandri M, Giavaresi G, Marcacci M, Hung CT, Tampieri A. Intrinsically superparamagnetic Fe-hydroxyapatite nanoparticles positively influence osteoblast-like cell behaviour. J Nanobiotechnology. 2012; 10:1–10. [PubMed: 22221512]
33. Parelman M, Stoecker B, Baker A, Medeiros D. Iron restriction negatively affects bone in female rats and mineralization of hFOB osteoblast cells. Exp Biol Med Maywood NJ. 2006; 231:378–386.
34. Pareta RA, Taylor E, Webster TJ. Increased osteoblast density in the presence of novel calcium phosphate coated magnetic nanoparticles. Nanotechnology. 2008; 19:265101. [PubMed: 21828670]
35. Ravaglioli, A., Krajewski, A. Bioceramics. Dordrecht: Springer Netherlands; 1992. p. 422at <http://link.springer.com/10.1007/978-94-011-2336-5>
36. Rout SR, Behera B, Maiti TK, Mohapatra S. Multifunctional magnetic calcium phosphate nanoparticles for targeted platin delivery. Dalton Trans Camb Engl 2003. 2012; 41:10777–10783.
37. Roy M, Bandyopadhyay A, Bose S. Induction plasma sprayed Sr and Mg doped nano hydroxyapatite coatings on Ti for bone implant. J Biomed Mater Res B Appl Biomater. 2011; 99B: 258–265.
38. Roy M, Fielding GA, Beyenal H, Bandyopadhyay A, Bose S. Mechanical, In vitro Antimicrobial, and Biological Properties of Plasma-Sprayed Silver-Doped Hydroxyapatite Coating. ACS Appl Mater Interfaces. 2012; 4:1341–1349. [PubMed: 22313742]
39. Roy M, Fielding G, Bandyopadhyay A, Bose S. Effects of Zinc and Strontium Substitution in Tricalcium Phosphate on Osteoclast Differentiation and Resorption. Biomater Sci. 2013; 1
40. Samavedi S, Whittington AR, Goldstein AS. Calcium phosphate ceramics in bone tissue engineering: a review of properties and their influence on cell behavior. Acta Biomater. 2013; 9:8037–8045. [PubMed: 23791671]
41. Seeley Z, Bandyopadhyay A, Bose S. Tricalcium phosphate based resorbable ceramics: Influence of NaF and CaO addition. Mater Sci Eng C. 2008; 28:11–17.

Author Manuscript Author Manuscript Author Manuscript Author Manuscript

42. Silva CC, Vasconcelos IF, Sombra ASB, Valente MA. Magnetic properties study on Fe-doped calcium phosphate. Phys Scr. 2009; 80:55706.
43. Tarafder S, Davies NM, Bandyopadhyay A, Bose S. 3D printed tricalcium phosphate bone tissue engineering scaffolds: effect of SrO and MgO doping on in vivo osteogenesis in a rat distal femoral defect model. Biomater Sci. 2013; 1:1250–1259. [PubMed: 24729867]
44. Tarafder S, Dernell WS, Bandyopadhyay A, Bose S. SrO- and MgO-doped microwave sintered 3D printed tricalcium phosphate scaffolds: Mechanical properties and in vivo osteogenesis in a rabbit model. J Biomed Mater Res B Appl Biomater. 2015; 103:679–690. [PubMed: 25045131]
45. Tran N, Hall D, Webster TJ. Mechanisms of enhanced osteoblast gene expression in the presence of hydroxyapatite coated iron oxide magnetic nanoparticles. Nanotechnology. 2012; 23:455104. [PubMed: 23064042]
46. Tran N, Webster TJ. Increased osteoblast functions in the presence of hydroxyapatite-coated iron oxide nanoparticles. Acta Biomater. 2011; 7:1298–1306. [PubMed: 20937416]
47. Tsay J, Yang Z, Ross FP, Cunningham-Rundles S, Lin H, Coleman R, Mayer-Kuckuk P, Doty SB, Grady RW, Giardina PJ, Boskey AL, Vogiatzi MG. Bone loss caused by iron overload in a murine model: importance of oxidative stress. Blood. 2010; 116:2582–2589. [PubMed: 20554970]
48. Vahabzadeh S, Hack VK, Bose S. Lithium-doped β-tricalcium phosphate: Effects on physical, mechanical and in vitro osteoblast cell-material interactions. J Biomed Mater Res B Appl Biomater. 2015; doi: 10.1002/jbm.b.33485
49. Vogiatzi MG, Macklin EA, Fung EB, Cheung AM, Vichinsky E, Olivieri N, Kirby M, Kwiatkowski JL, Cunningham M, Holm IA, Lane J, Schneider R, Fleisher M, Grady RW, Peterson CC, Giardina PJ, Thalassemia Clinical Research Network. Bone disease in thalassemia: a frequent and still unresolved problem. J Bone Miner Res Off J Am Soc Bone Miner Res. 2009; 24:543–557.
50. Wu Y, Jiang W, Wen X, He B, Zeng X, Wang G, Gu Z. A novel calcium phosphate ceramic-magnetic nanoparticle composite as a potential bone substitute. Biomed Mater Bristol Engl. 2010; 5:15001.
51. Yamamoto Y, Ohsaki Y, Goto T, Nakasima A, Iijima T. Effects of static magnetic fields on bone formation in rat osteoblast cultures. J Dent Res. 2003; 82:962–966. [PubMed: 14630895]
52. Yang Q, Jian J, Abramson SB, Huang X. Inhibitory effects of iron on bone morphogenetic protein 2-induced osteoblastogenesis. J Bone Miner Res Off J Am Soc Bone Miner Res. 2011; 26:1188–1196.
53. Yin X, Stott MJ, Rubio A. α – and β -tricalcium phosphate: A density functional study. Phys Rev B. 2003; 68
54. Yoshida K, Hyuga H, Kondo N, Kita H, Sasaki M, Mitamura M, Hashimoto K, Toda Y. Substitution Model of Monovalent (Li, Na, and K), Divalent (Mg), and Trivalent (Al) Metal Ions for β-Tricalcium Phosphate. J Am Ceram Soc. 2006; 89:688–690.
55. Yuge L, Okubo A, Miyashita T, Kumagai T, Nikawa T, Takeda S, Kanno M, Urabe Y, Sugiyama M, Kataoka K. Physical stress by magnetic force accelerates differentiation of human osteoblasts. Biochem Biophys Res Commun. 2003; 311:32–38. [PubMed: 14575691]
56. Zhang L, Schlesinger ME, Brow RK. Phase Equilibria in the Fe2O3–P2O5 System. J Am Ceram Soc. 2011; 94:1605–1610.
57. National Osteoporosis Foundationat. What is Osteoporosis?. <http://nof.org/articles/7>
58. International Osteoporosis Foundationat. Facts and Statistics. <http://www.iofbonehealth.org/facts-statistics>
59. National Osteoporosis Foundationat. 54 Million Americans Affected by Osteoporosis and Low Bone Mass. <http://nof.org/news/2948>

Author Manuscript Author Manuscript Author Manuscript Author Manuscript

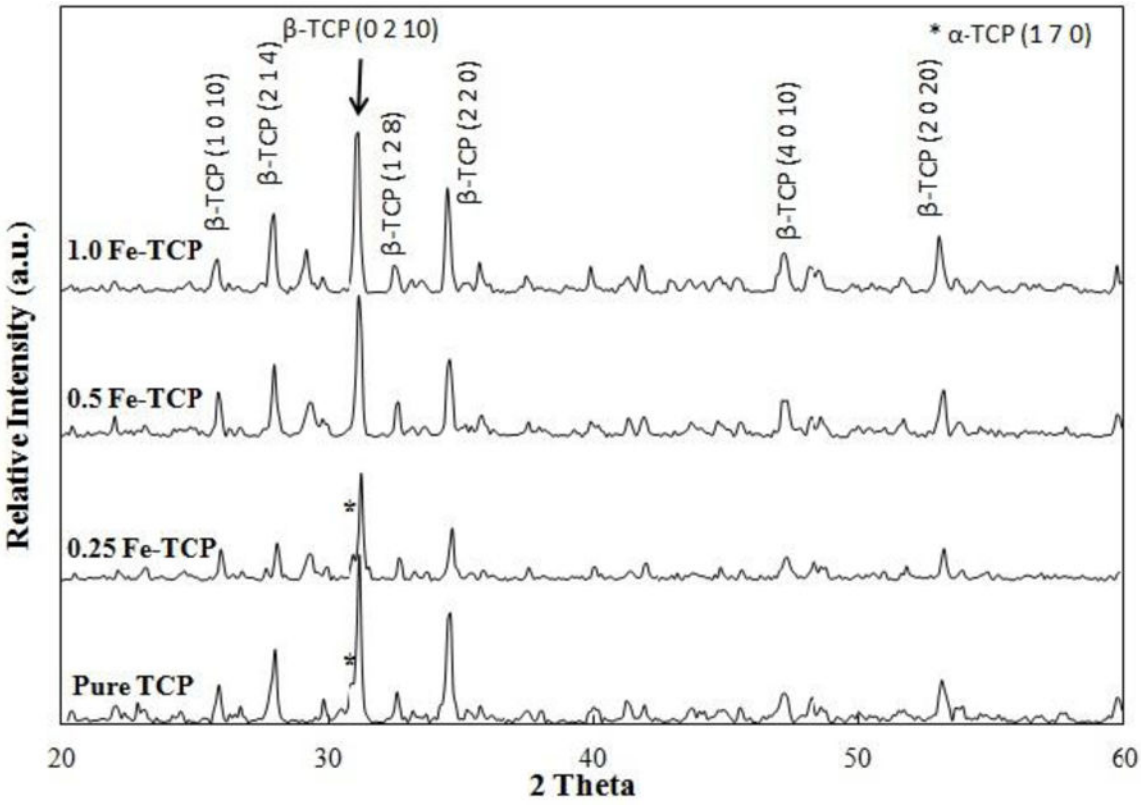

Figure 1.
XRD spectra of pure and Fe-doped TCPs sintered at 1250 °C.

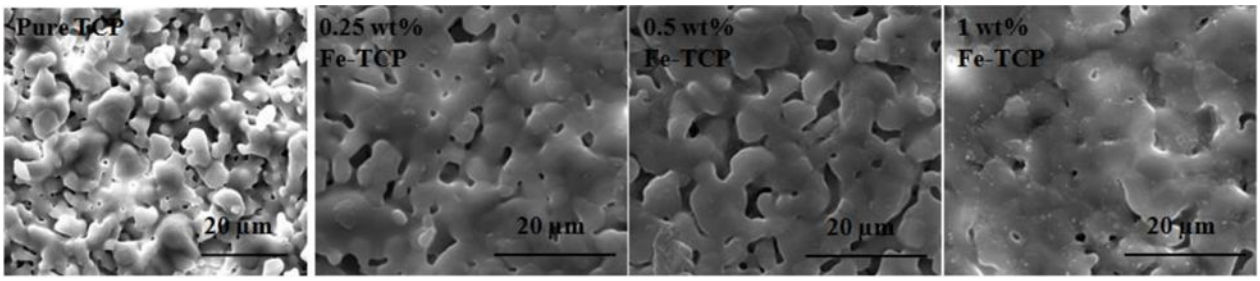

Figure 2.
SEM micrographs of pure and Fe-doped TCP samples after sintering at 1250 °C.

Author Manuscript Author Manuscript Author Manuscript Author Manuscript

Author Manuscript Author Manuscript Author Manuscript Author Manuscript

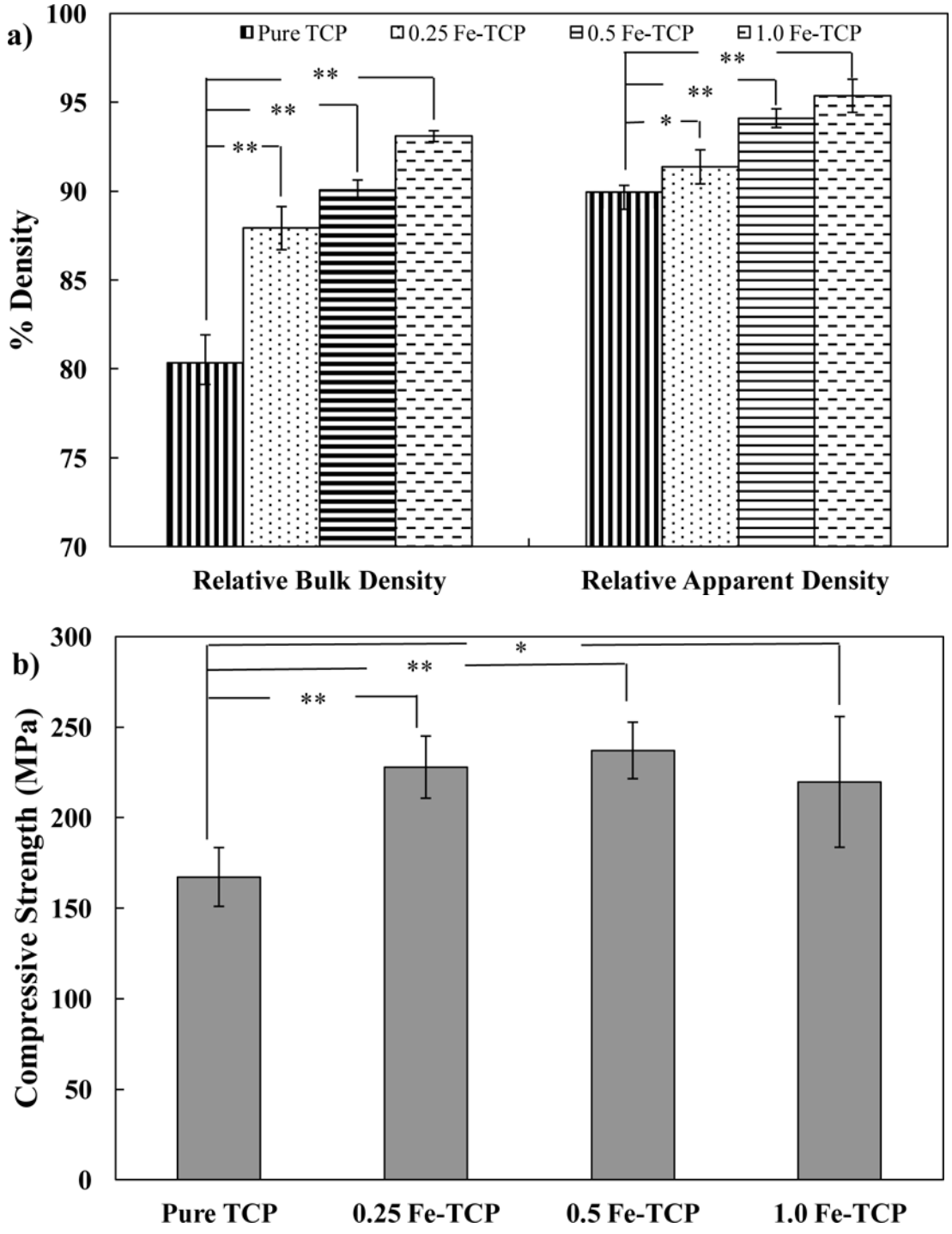

Figure 3.

a) Relative bulk and apparent densities, and b) Compressive strength of pure and Fe-doped TCP samples, sintered at 1250 °C, using cylindrical samples (7 mm diameter and 12 mm height). Data is presented as mean ± standard deviation (* $P < 0.05$ and ** $P<0.01$).

Author Manuscript Author Manuscript Author Manuscript Author Manuscript

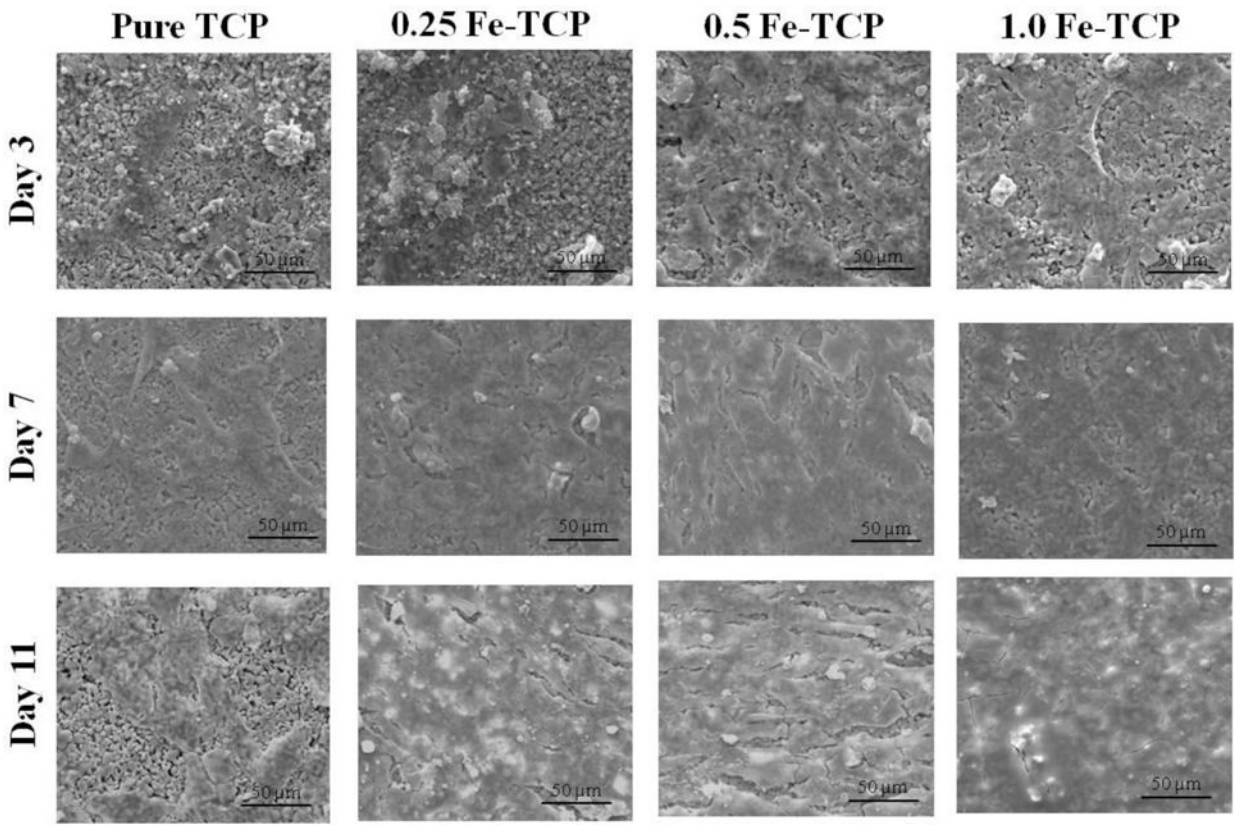

Figure 4.
hFOB cell morphology on pure and Fe-doped TCP samples after 3, 7, and 11 days of culture.

Author Manuscript Author Manuscript Author Manuscript Author Manuscript

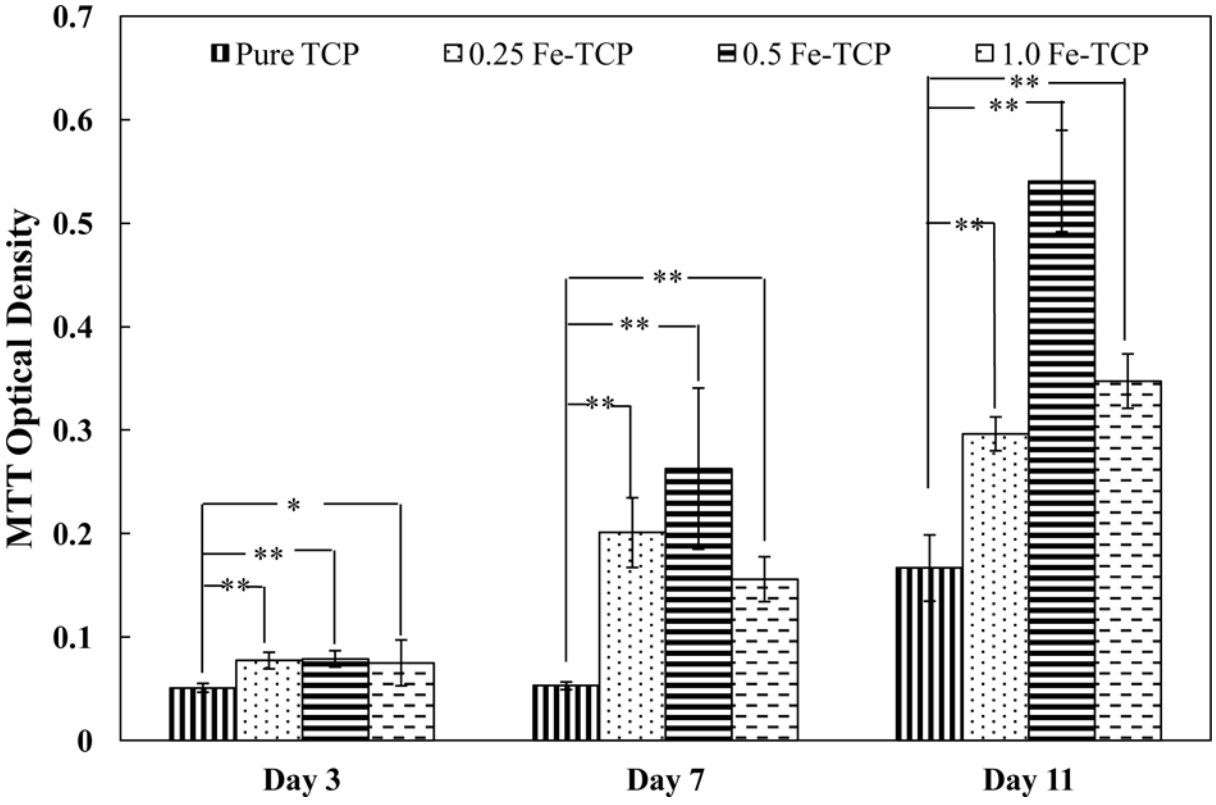

Figure 5.

hFOB optical cell density on pure and Fe-doped TCP disks (12 mm diameter and 2 mm thickness) after 3, 7, and 11 days of culture. Data is presented as mean ± standard deviation (* $P < 0.05$ and ** $P<0.01$).

Author Manuscript Author Manuscript Author Manuscript Author Manuscript

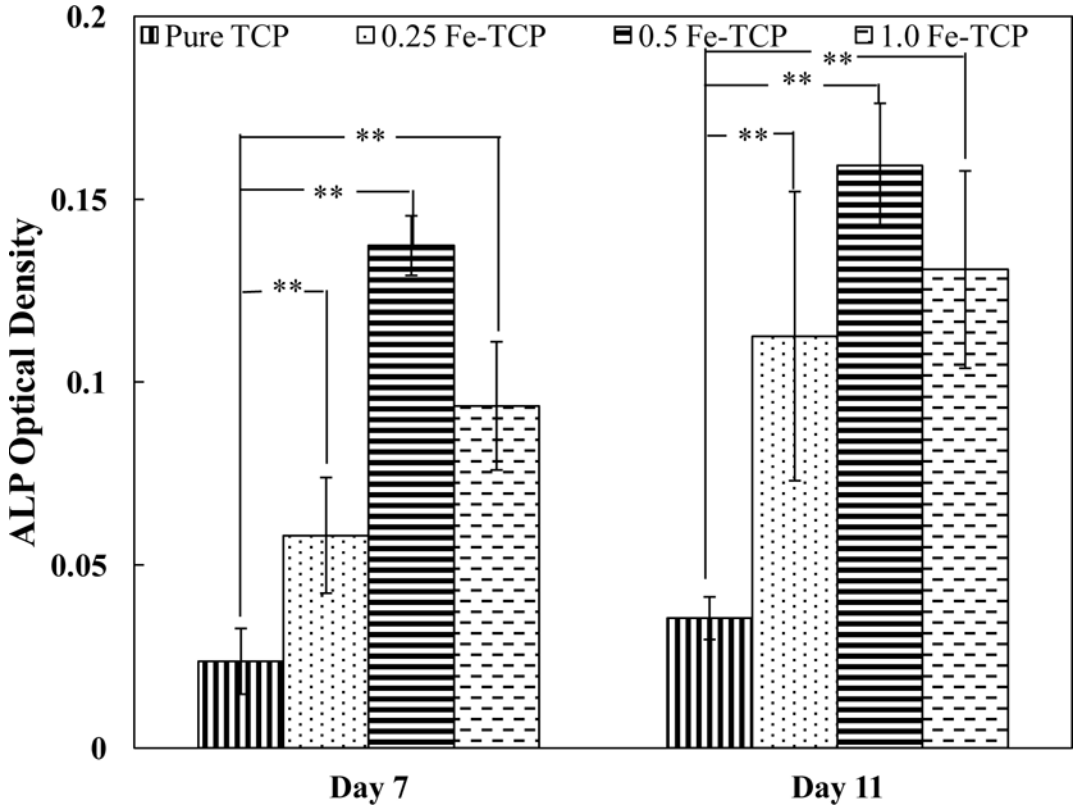

Figure 6.

ALP optical density on pure and Fe-doped TCP disks (12 mm diameter and 2 mm thickness) after 7 and 11 days of culture. Data is presented as mean ± standard deviation (* $P < 0.05$ and ** $P<0.01$).

Author Manuscript Author Manuscript Author Manuscript Author Manuscript

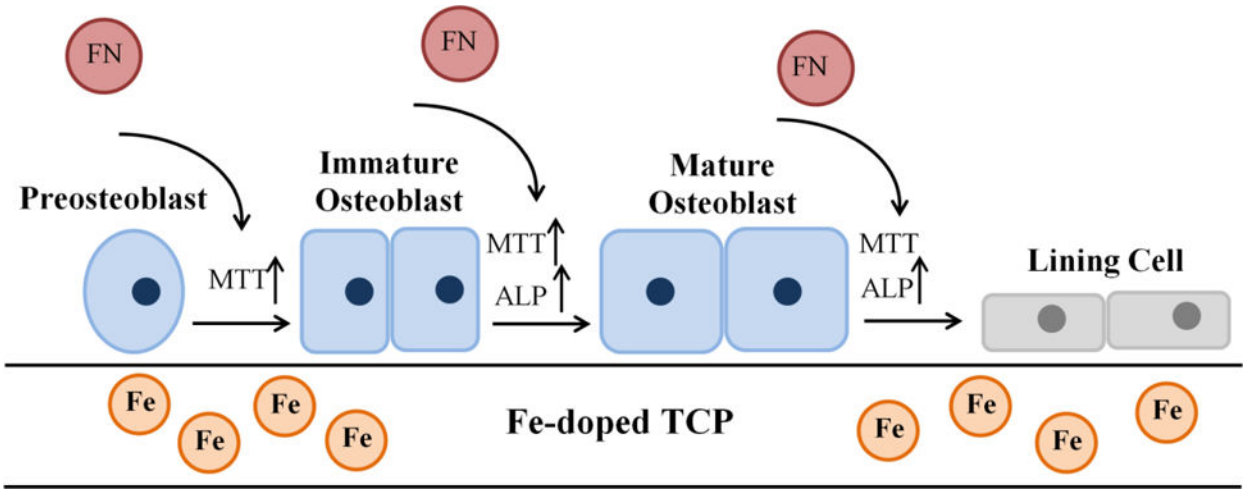

Figure 7.

Schematic presentation of cellular level mechanisms showing the effects of Fe dopant on proliferation, differentiation, and maturation of osteoblast cells.